Auger recombination in narrow-gap semiconductor superlattices incorporating antimony

C. H. Grein
Microphysics Laboratories and Department of Physics M/C 273, University of Illinois at Chicago, 845 West Taylor Street No. 2236, Chicago, Illinois 60607-7059

M. E. Flatté[a] and J. T. Olesberg
Department of Physics and Astronomy and Optical Science and Technology Center, University of Iowa, Iowa City, Iowa 52242

S. A. Anson
Optical Science and Technology Center and Department of Electrical and Computer Engineering, University of Iowa, Iowa City, Iowa 52242

L. Zhang
Department of Physics and Astronomy and Optical Science and Technology Center, University of Iowa, Iowa City, Iowa 52242

T. F. Boggess
Department of Physics and Astronomy, Optical Science and Technology Center, and Department of Electrical and Computer Engineering, University of Iowa, Iowa City, Iowa 52242

(Received 15 April 2002; accepted 20 September 2002)

A comparison is performed between measured and calculated Auger recombination rates for four different narrow-gap superlattices based on the InAs/GaSb/AlSb material system. The structures are designed for optical or electrical injection for mid-infrared laser applications, with wavelengths ranging from 3.4 to 4.1 μm. The electronic band structures are computed employing an accurate 14-band restricted basis set (superlattice $\mathbf{K}\cdot\mathbf{p}$) methodology that utilizes experimental information about the low-energy electronic structure of the bulk constituents. The superlattice band structures and their associated matrix elements are directly employed to compute Auger recombination rates. Varying amounts of Auger recombination suppression are displayed by the various superlattices as compared to bulk mid-infrared systems. The greatest disagreement between theory and experiment is shown for the structure predicted to have the most Auger suppression, suggesting the suppression is sensitive either to theoretical or growth uncertainties. © *2002 American Institute of Physics.*
[DOI: 10.1063/1.1521255]

I. INTRODUCTION

Semiconductor-based infrared technology for light wavelengths beyond 2 μm is leading to applications in several fields, including remote pollution monitoring and commercial night vision equipment. Intense materials development has resulted in some devices, notably those detectors based on $Hg_{1-x}Cd_xTe$, which operate near theoretical limits.[1] However, even when operating at theoretical limits, many present day devices require substantial cooling. For lasers whose operation is based on interband transitions, intrinsic Auger recombination causes most of the heating and carrier loss. For interband detectors, intrinsic Auger recombination dominates the dark current, and thus the noise. In the intrinsic Auger recombination process the energy and momentum of a recombining electron–hole pair are transferred to a third carrier, rather than to a photon. Such processes are particularly important in small band gap materials, both because of higher thermal carrier concentrations (Auger recombination rates increase rapidly with carrier density) and because satisfying the momentum and energy conservation requirements of the process is easier when the energy transfer in the process is smaller.

As the Auger process depends sensitively on the material's electronic structure, the flexibility associated with semiconductor heterostructures has spawned a variety of strategies for designing materials with reduced Auger recombination rates. The first significant strategies for reducing the probability of Auger recombination transitions in heterostructure lasers[2,3] were based on reducing the threshold carrier density and matching the conduction electron and valence hole masses (which makes energy and momentum conservation in the Auger process more difficult).[4] Subsequent strategies have been developed over the past decade[5–10] which employ band structure engineering in strained-layer superlattices to remove possible final states in Auger transitions, and thereby decrease Auger recombination rates. The utility of these strategies for superlattices with band gaps of ~10 μm was shown in Refs. 11 and 12, in which the Auger rates were measured and calculated to be as much as 2 orders of magnitude smaller in well-designed superlattices than in

[a]Author to whom correspondence should be addressed; electronic mail: michael-flatte@uiowa.edu

 © 2002 American Institute of Physics

Downloaded 19 Jan 2005 to 128.255.34.225. Redistribution subject to AIP license or copyright, see http://jap.aip.org/jap/copyright.jsp

TABLE I. Four structures considered in this article, their band gap, and the reference where the structure is described.

Structure	Band gap (μm)	Structure	Ref.
(a)	4.1	17 Å InAs/26 Å $Ga_{0.74}In_{0.26}Sb$/17 Å InAs/43 Å AlSb	15
(b)	4.1	15 Å InAs/25 Å $Ga_{0.6}In_{0.4}Sb$/15 Å InAs/39 Å $Al_{0.30}In_{0.28}Ga_{0.42}As_{0.5}Sb_{0.5}$	14
(c)	4.1	33 Å $Ga_{0.65}In_{0.35}Sb$/20 Å InAs/40 Å AlSb	
(d)	3.4	18 Å InAs/21 Å $AlAs_{0.15}Sb_{0.85}$/18 Å InAs/25 Å $Ga_{0.6}In_{0.4}Sb$/ 18 Å InAs/21 Å $Al_{0.15}Sb_{0.85}$/18 Å InAs (27 Å $Al_{0.6}Ga_{0.4}Sb$/11 Å InAs)$_{4.5}$	10

bulk systems with the same band gap. Suppression of Auger recombination rates in type-II heterostructures by roughly a factor of 4 in the mid-wavelength infrared (MWIR) (relative to type-I heterostructures) has been observed,[13] however this suppression appears to be largely due to balancing the conduction and valence band masses rather than final-state structure.[9]

Although the above strategies for reducing Auger recombination can be formulated based on qualitative considerations, to be of most utility accurate calculations of electronic structure and Auger recombination rates for superlattices should be available to correlate specific superlattice structures with optimal Auger rates. These calculations can assist device design by providing ideal limits and by differentiating between competing material systems. The principal difficulty in the computation of Auger recombination rates is the integration over the wave vectors of all possible initial and final states in the Brillouin zone (subject to energy and momentum conservation constraints). Their computation was pioneered by Beattie and Landsberg[4] with the assumptions of parabolic bands and constant overlap matrix elements. These assumptions permitted the number of integrals requiring numerical evaluation to be reduced to only one. The early expressions obtained by Beattie and Landsberg are still employed often today, however they prove in many cases to be poor approximations, particularly in superlattices. The energy bands of superlattices are highly nonparabolic and the matrix elements depend sensitively on carrier momentum. Inaccurate approximations for the band energies are particularly problematic due to the resulting exponential errors in occupation probabilities. However, the use of realistic electronic band structures for superlattices has until recently been computationally prohibitive. Direct comparisons of accurate theoretical calculations (without free parameters) with experimental measurements of Auger recombination rates are very rare for narrow band gap systems where the final states for the third carrier have nontrivial structure. Success has been reported for a long-wavelength infrared InAs/GaInSb superlattice[11,14] and for a MWIR InAs/GaInSb/AlGaInAsSb superlattice.[14]

This article explores theoretically Auger recombination in four different Sb-based mid-infrared heterostructure materials at $T = 300$ K, discussing Auger recombination suppression strategies and their effectiveness. Direct comparisons with experiment are presented to demonstrate the accuracy of present-day band structure and Auger recombination computational tools. The electronic structure and carrier–carrier scattering matrix elements are evaluated with a low-energy restricted-basis set calculation based on fourteen bulk bands (six bonding p-like states, two antibonding s-like states, and six antibonding p-like states). The recombination rates reported are calculated employing these band structures and matrix elements.

The four structures considered are tabulated in Table I. Structure (a) is a "W" laser grown on a GaSb substrate at the Naval Research Labs.[15] Time resolved photoluminescence measurements[16] were performed to obtain the recombination rates. This structure has been successfully employed as the active region of optically pumped lasers emitting in the MWIR.[15,17] Structures (b) and (d) were grown on a GaSb substrate with a GaSb cap layer at the University of Iowa[14] and structure (c) was grown at the University of Houston. The carrier recombination rates for (b), (c) and (d) were determined via differential transmission measurements[18] as described in Ref. 14. Each of the structures is a type-II heterostructure, which should show some suppression of Auger recombination relative to bulk structures because of the improved matching of conduction and valence band-edge densities of states (or, approximately, effective masses). The first three structures, however, show only marginal suppression of Auger recombination at 300 K through final-state optimization, whereas the fourth structure is predicted to have significant suppression of Auger recombination at 300 K. Agreement between theory and experiment is excellent for the first three structures, but not for the fourth, indicating that Auger suppression is sensitive to theoretical or growth uncertainties.

II. METHODS

The methodology for calculating the electronic band structures of the four systems listed above is closely related to the well-known **k·p** methodology, which is commonly based on eight bulk bands. The 14-band basis we use here includes the higher-lying antibonding p states in addition to the common eight bands (bonding p states and antibonding s states). Input parameters for this method are determined from the energy levels, effective masses, and g factors of the bulk constituents, as well as the valence band offsets between layers. The employed parameters are mainly extracted from

Downloaded 19 Jan 2005 to 128.255.34.225. Redistribution subject to AIP license or copyright, see http://jap.aip.org/jap/copyright.jsp

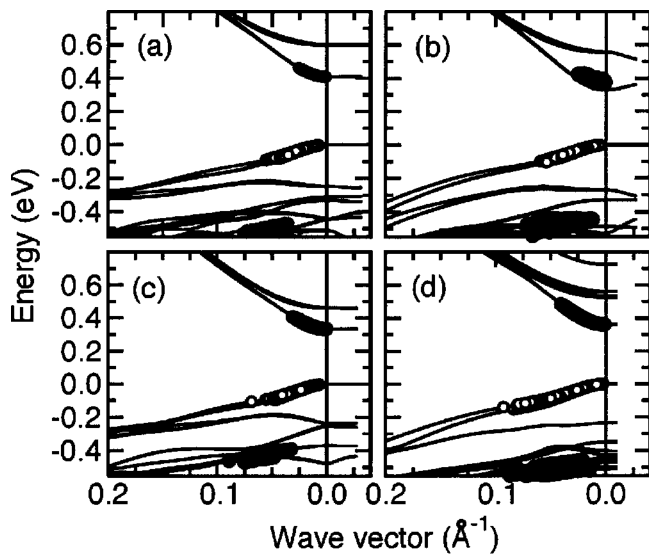

FIG. 1. Most probable hole Auger processes for the four structures considered at 300 K. The superlattice bands are plotted in the growth axis direction (right of vertical line) and in-plane direction (left of vertical line). Holes are indicated by hollow circles and electrons by solid circles. The electron and hole positions are plotted superimposed on the curves of the computed electronic band structure and are plotted only as a function of their in-plane momentum component, so they do not always lie on the curves. The carrier concentrations are n=p= (a) 2×10^{17} cm^{-3}, (b) 5×10^{17} cm^{-3}; (c) 5×10^{17} cm^{-3}, and (d) 3×10^{17} cm^{-3}.

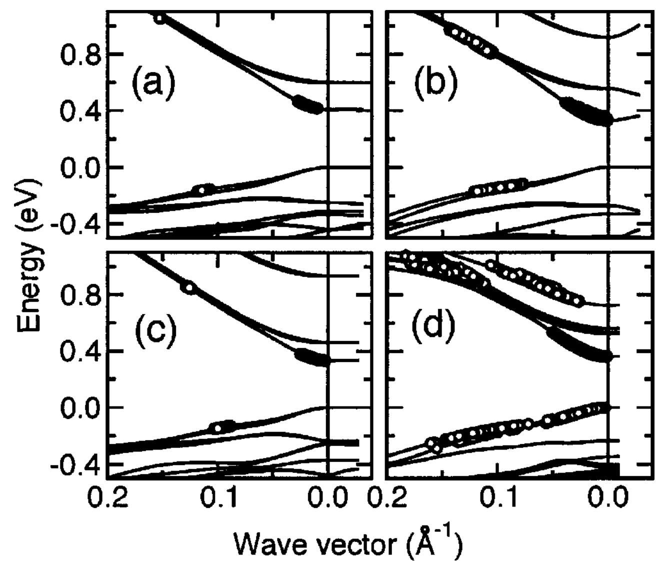

FIG. 2. Same as Fig. 1, but for electron Auger processes.

Ref. 19 and are fully reported in Ref. 20. This formalism has proven to be very accurate in the calculation of optical absorption,[21,22] linewidth enhancement factors,[23] and spin coherence times[24] (in addition to the previously mentioned carrier lifetimes) for similar type-II Sb-based multilayer structures. The theoretical results presented here for one of the superlattices are slightly different from those in Ref. 14 because a 14-band calculation is used rather than an eight-band one.

The highly nonparabolic band structures and momentum matrix elements are used directly as input for the computation of Auger lifetimes. They are input into the Auger rate computations in the form of look-up tables with a mesh spacing of 0.002 Å^{-1}. The principal methods employed are discussed in Ref. 8, and have been extended to include the effects of superlattice Umklapp processes.[14] Umklapp processes are negligible in bulk direct gap systems.[25] However, due to the large size of the superlattice unit cells and hence the small size of reciprocal lattice vectors in the growth-axis direction, Umklapp processes have been shown to contribute approximately half of the total rate of Auger recombination in superlattices.[14] The transition matrix elements are evaluated using a statically screened Coulomb interaction and first order $\mathbf{K}\cdot\mathbf{p}$ for the wave function overlaps. The multidimensional **K** space integrals are evaluated employing an adaptive mesh Monte Carlo algorithm.

Plots of the most probable **K** space locations of electrons and holes before undergoing Auger transitions are helpful in designing superlattices which suppress Auger recombination. Those presented in this article (in Figs. 1 and 2 to be described below) were produced by selecting the Auger processes which contribute the most to the total recombination rate. The electron and hole states (on the **K**-space mesh described above) involved in those processes are then plotted on the superlattice band structure. The transitions shown account for more than 99% of the total Auger recombination rate. For each of the four systems considered here, the electron and hole densities (defined as the average densities over the entire superlattice period) were in the range of low- to mid-10^{17} cm^{-3} for the computation of the most probable locations of the carriers. This permits the direct comparison of Auger transitions of the systems with similar carrier concentrations.

The measurements of recombination rates on these systems were performed either with time-resolved photoluminescence (PL) upconversion or differential transmission. Pulses of 140 fs duration and photon energy 1.476 eV from a mode-locked Ti:sapphire laser were used to excite electron–hole pairs in the structures. For the differential transmission measurements 170 fs probe pulses from a synchronously pumped optical parametric oscillator were used to probe the transmission at 0.349 eV (near the absorption edge). For the PL upconversion measurements a delayed piece of the pump pulse (gating pulse) was mixed with the mid-infrared PL in a nonlinear crystal, and the upconverted light intensity was detected. For both methods the signal increases as the initially hot carriers relax to the band edge states and then decays as the carriers recombine. Measurements of the decay of the signal can then be correlated with the decay of the carrier distribution itself.

Experimental recombination rate data as a function of carrier density are typically fitted to the form

$$R=A+Bn+Cn^2, \qquad (1)$$

where R is the recombination rate per electron–hole pair, and n is the carrier density. The fitting constant A represents the rate of Shockley–Read–Hall recombination, B measures the radiative recombination rate, and C the Auger recombination rate. In the four samples considered here, the radiative recombination rate was calculated in every case to be at least

Downloaded 19 Jan 2005 to 128.255.34.225. Redistribution subject to AIP license or copyright, see http://jap.aip.org/jap/copyright.jsp

one order of magnitude longer than the Auger recombination rate over the considered ranges of carrier density. Hence radiative recombination is not considered further. It has been previously noted[26] that the rate of Auger recombination is expected to saturate when the involved carriers become degenerate, with the rate approaching a linear dependence on the carrier density. Without careful analysis this saturation can generate a spurious result for the radiative coefficient B if Eq. (1) is used. Hence, the experimental data here were analyzed by fitting the recombination rate as a function of carrier density to the expression

$$R=A+Cn^2/(1+n/n_0), \tag{2}$$

where n_0 is a measure of the carrier density for the onset of saturated behavior.

III. RESULTS AND DISCUSSION

We begin by comparing for each of the four structures the nature of the states involved in Auger recombination. Figure 1 shows the states involved in the most probable hole Auger processes in each of the four structures (a)–(d), and Fig. 2 shows the states involved in the most probable electron Auger processes. Here "hole" Auger recombination indicates a process where the energy and momentum of the recombining electron–hole pair are transferred to a hole, and "electron" Auger recombination when the transfer is to an electron. The band structures are plotted in the growth-axis direction to the right and in the in-plane direction to the left. Electron states involved in the process are indicated by solid circles, and hole states by hollow circles. In both cases the positions of the electrons and holes are superimposed on the electronic band structure. The most probable transitions are plotted as a function of the carrier's in-plane momentum component only, and thus do not always lie on the curves. For all four systems the hole Auger processes dominate the overall Auger recombination rate at 300 K.

Figure 3 shows the observed and calculated recombination rates for the four systems and Table II summarizes the fits of Eq. (2) to the experimentally measured density dependence of the recombination rate. The Shockley–Read–Hall times of each of these are comparable, ranging from 2.5 to 10 ns. Saturation of the experimental Auger recombination rate (indicated by a smaller n_0 in Table II and a more linear behavior in Fig. 3) is evident in both structures (c) and (d) around the middle of the plotted range, whereas in (a) and (b) saturation is not visible. Saturation of the hole Auger rate (which dominates) requires the holes to become degenerate, so these measurements indicate that the holes have not become degenerate for the densities probed in (a) and (b), whereas they have in (c) and (d). The theoretical Auger recombination, however, does not saturate significantly for any of the four structures.

Both the Auger coefficients and the saturation densities show substantial apparent variation between theory and experiment, despite the apparent good agreement of the plots of the recombination rates (Fig. 3) for structures (a)–(c). This can occur because the Auger coefficient is principally determined by the low-density region of the curves, whereas the

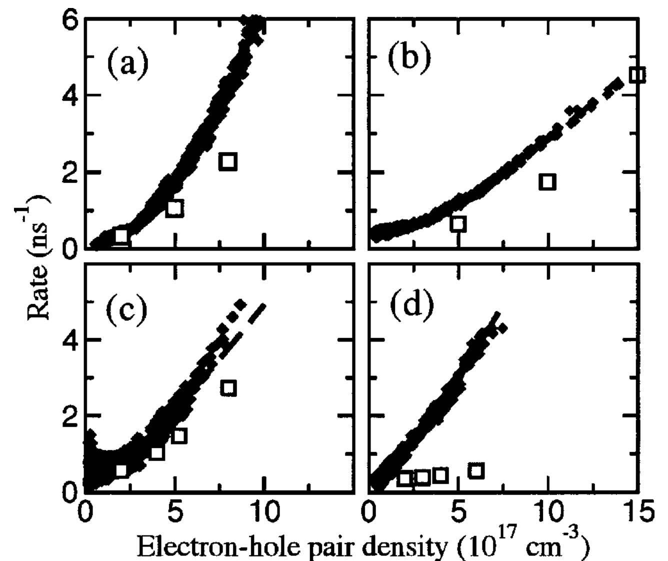

FIG. 3. Experimental (solid diamonds) and computed (hollow squares) total recombination rates per electron–hole pair for the four systems. The dashed lines are fits of the experimental data to Eq. (2).

saturation density is governed by the higher-density region. Thus comparisons of Auger coefficients for such structures must be done with care. A more robust comparison can be made using the Auger rate at a given density, in this case (Table II) the rates for a density of 10^{18} cm^{-3}. The theoretical and experimental rates at that density are within a factor of 2 for structures (a)–(c).

We focus on the density of 10^{18} cm^{-3} because that is close to the optimal lasing density for the first three structures (a)–(c). At these densities the Auger recombination rate is over 1 order of magnitude greater than the Shockley–Read–Hall rate. Thus the focus on the Auger recombination rate is justified for these systems. At the density of 10^{18} cm^{-3} the four structures have an Auger rate that is smaller than the 9 ns^{-1} calculated for bulk 4.1 μm $InAs_{0.91}Sb_{0.09}$. The nature of the band-edge electronic structure of these four superlattices forces more of the energy and momentum conserving Auger transitions to involve near-band-edge carriers deep in the tails of their Fermi distributions, and hence in regions of lower occupation probability.

The fourth structure (d) is the optimized structure, even though its measured Auger coefficient is larger than that of the other three. This peculiarity occurs because Auger coefficients are not very good benchmarks for structures which differ substantially in their *optical* properties.[27] A simple indication of how Auger coefficients can be misleading is given by a multiple quantum well material. If the optically active well thickness is kept the same, and the barrier thickness is increased, the Auger coefficient increases proportionally to the total thickness of the well and barrier squared. However the net material gain per unit recombination current remains the same. The first three structures have similar material gains for similar carrier densities, and the true figure of merit (net material gain per unit recombination current)[28] can be fairly represented by the Auger coefficient. Structure (d) is a much thicker multilayer structure than (a)–(c), more like a sophisticated quantum well, and it reaches its maximal figure

Downloaded 19 Jan 2005 to 128.255.34.225. Redistribution subject to AIP license or copyright, see http://jap.aip.org/jap/copyright.jsp

TABLE II. Measured and theoretical parameters that describe the density dependence of the recombination rate according to Eq. (2): A the Shockley–Read–Hall recombination rate, C the low-density Auger recombination coefficient, and n_0, the saturation density for Auger recombination. τ is the total lifetime, whereas τ_e is the electron Auger lifetime and τ_h is the hole Auger lifetime. All quoted lifetimes are for a carrier concentration of 10^{18} cm^{-3}.

Structure	A (ns^{-1})	C (10^{-27} cm^6 s^{-1})		n_0 (10^{18} cm^{-3})		τ^{-1} (ns^{-1})		τ_e^{-1} (ns^{-1})	τ_h^{-1} (ns^{-1})
	Exp	Exp	Theor.	Exp.	Theor.	Exp.	Theor.	Theor	Theor
(a)	0.11	7.2	4.1	7.1	3.1	6.4	3.2	0.8	2.3
(b)	0.41	4.5	4.6	1.2	1.1	2.9	2.8	0.4	2.0
(c)	0.40	15.4	4.4	0.42	4.1	5.0	3.9	1.0	2.5
(d)	0.31	26	0.9	0.35	1.8	7.1	0.9	0.01	0.6

of merit at a carrier density of merely 3.4×10^{17}cm^{-3}. As a result, the net material gain per unit recombination current is predicted to be one order of magnitude greater for system (d) than for any of the other three structures, resulting in a predicted threshold current density one order of magnitude smaller.

The agreement between theoretical and observed Auger rates at the optimal carrier density for lasing is no worse than a factor of 2 for the first three systems, suggesting the validity and accuracy of the band structure and Auger rate computational methodologies. However, for the fourth structure there is significant disagreement. Even with this disagreement, however, the net material gain per unit recombination current of (d) is measured to be a factor of 2 superior to that of structure (b), which had the previous material record.[29]

There are several possible sources of the discrepancy between theory and experiment for structure (d). The presence of Auger suppression in the predicted electronic structure of (d) is sensitive to the precise layer thicknesses of the constituent materials.[10] Hence errors either in the theoretical calculations of the band structure, or errors in growth may lead to less suppression than expected. The multitude of bands involved in the sophisticated thick structure (d) make convergence of the Monte Carlo calculations for the Auger rates delicate. Also, other Auger processes which are typically of less importance in less optimized structures may now emerge to dominate, including defect-assisted Auger or phonon-assisted Auger. Detailed studies of trends in carrier lifetimes for the broken-gap quantum well of structure (d) would be required to clarify the origin of the discrepancy.

IV. SUMMARY

The reported results indicate considerable variability in 300 K Auger coefficients in four mid-wavelength infrared Sb-based material systems. This is associated with band structure effects modifying locations in **K** space where energy and momentum conserving Auger transitions can occur. Structures that are not predicted to have significant Auger suppression due to the elimination of final states for the process are observed to exhibit excellent agreement between predicted and observed Auger recombination rates. The structure (d), which is predicted to have substantially reduced Auger recombination rates at 300 K, is observed to exhibit some significant Auger suppression, but not as much as predicted. Further studies of structures like that of (d) would clarify the relative contributions to this discrepancy of theoretical uncertainty in electronic structures, statistical error in the Auger rate calculations, theoretical uncertainty in the importance of higher-order Auger processes, and experimental uncertainty in growth.

ACKNOWLEDGMENTS

This work was supported by the National Science Foundation (Grant Nos. ECS-0000556, ECS-9707799, and ECS-9406690), and by the U.S. Air Force Research Laboratory Directed Energy Directorate, Kirtland AFB New Mexico 87117-5776 (Contract Nos. F29601-00-C-0005 and F29601-97-C-0041). The authors are grateful to M. J. Yang and J. Meyer for samples of type (a), T. C. Hasenberg for samples of type (b) and (d), and C. H. Lin for samples of type (c).

[1] W. E. Tennant and C. Cabelli, Mater. Res. Soc. Symp. Proc. **484**, 221 (1998).
[2] A. R. Adams, Electron. Lett. **22**, 249 (1986).
[3] E. Yablonovitch and E. O. Kane, J. Lightwave Technol. **4**, 504 (1986).
[4] A. R. Beattie and P. T. Landsberg, Proc. R. Soc. London **249**, 16 (1959).
[5] C. H. Grein, P. M. Young, and H. Ehrenreich, Appl. Phys. Lett. **61**, 2905 (1992).
[6] P. M. Young, C. H. Grein, H. Ehrenreich, and R. H. Miles, J. Appl. Phys. **74**, 4774 (1993).
[7] M. E. Flatté, C. H. Grein, H. Ehreinreich, R. H. Miles, and H. Cruz, J. Appl. Phys. **78**, 4552 (1995).
[8] C. H. Grein, P. M. Young, M. E. Flatté, and H. Ehrenreich, J. Appl. Phys. **78**, 7143 (1995).
[9] M. E. Flatté and C. H. Grein, Opt. Express **2**, 131 (1998).
[10] J. T. Olesberg, M. E. Flatté, T. C. Hasenberg, and C. H. Grein, J. Appl. Phys. **89**, 3283 (2001).
[11] E. R. Youngdale, J. R. Meyer, C. A. Hoffman, F. J. Bartoli, C. H. Grein, P. M. Young, H. Ehrenreich, R. H. Miles, and D. H. Chow, Appl. Phys. Lett. **64**, 3160 (1994).
[12] C. M. Ciesla *et al.*, J. Appl. Phys. **80**, 2994 (1996).
[13] J. R. Meyer *et al.*, Appl. Phys. Lett. **73**, 2857 (1998).
[14] M. E. Flatté, C. H. Grein, T. C. Hasenberg, S. A. Anson, D.-J. Jang, J. T. Olesberg, and T. F. Boggess, Phys. Rev. B **59**, 5745 (1999).
[15] W. W. Bewley *et al.*, Appl. Phys. Lett. **73**, 3833 (1998).
[16] D.-J. Jang, M. E. Flatté, C. H. Grein, J. T. Olesberg, T. C. Hasenberg, and T. F. Boggess, Phys. Rev. B **58**, 13047 (1998); D.-J. Jang *et al.*, Appl. Phys. Lett. **70**, 1125 (1997).
[17] W. W. Bewley *et al.*, Appl. Phys. Lett. **74**, 1075 (1999).
[18] S. W. McCahon *et al.*, Appl. Phys. Lett. **68**, 2135 (1996).
[19] O. Madelung, in *Semiconductors, Group IV Elements and III-V Compounds*, edited by K. H. Helluege and O. Madelung, Landolt-Börnstein, New Series, Group III, Vol. 17, Pt. A (Springer, Berlin, 1982).
[20] W. H. Lau, J. T. Olesberg, and M. E. Flatté (unpublished).
[21] J. T. Olesberg, S. A. Anson, S. W. McCahon, M. E. Flatté, T. F. Boggess,

Downloaded 19 Jan 2005 to 128.255.34.225. Redistribution subject to AIP license or copyright, see http://jap.aip.org/jap/copyright.jsp

D. H. Chow, and T. C. Hasenberg, Appl. Phys. Lett. **72**, 229 (1998).
[22] W. H. Lau and M. E. Flatté, Appl. Phys. Lett. **80**, 1683 (2002).
[23] S. A. Anson, J. T. Olesberg, M. E. Flatté, T. C. Hasenberg, and T. F. Boggess, J. Appl. Phys. **86**, 713 (1999).
[24] J. T. Olesberg, W. H. Lau, M. E. Flatté, C. Yu, E. Altunkaya, E. M. Shaw, T. C. Hasenberg, and T. F. Boggess, Phys. Rev. B **64**, 201301(R) (2001).
[25] S. Brand and R. A. Abram, J. Phys. C **17**, L571 (1984).
[26] A. Haug, in *Proceedings of 13th International Conference on the Physics of Semiconductors,* edited by F. G. Fumi (North-Holland, New York, 1976), p. 1106.
[27] M. E. Flatté, J. T. Olesberg, S. A. Anson, T. F. Boggess, T. C. Hasenberg, R. H. Miles, and C. H. Grein, Appl. Phys. Lett. **70**, 3212 (1997).
[28] J. T. Olesberg, M. E. Flatté, B. J. Brown, C. H. Grein, T. C. Hasenberg, S. A. Anson, and T. F. Boggess, Appl. Phys. Lett. **74**, 188 (1999).
[29] T. C. Hasenberg, P. S. Day, E. M. Shaw, D. J. Magarrell, J. T. Olesberg, C. Yu, T. F. Boggess, and M. E. Flatté, J. Vac. Sci. Technol. B **18**, 1623 (2000).

Downloaded 19 Jan 2005 to 128.255.34.225. Redistribution subject to AIP license or copyright, see http://jap.aip.org/jap/copyright.jsp